Intramural wave propagation in cardiac tissue: Asymptotic solutions and cusp waves

O. Bernus, M. Wellner, and A. M. Pertsov
Department of Pharmacology, SUNY Upstate Medical University, Syracuse, New York 13210, USA
(Received 10 June 2004; revised manuscript received 27 August 2004; published 27 December 2004)

The cardiac muscle is well known to conduct electric impulses anisotropically, showing a larger conduction velocity along than across fibers. Fiber orientation is not uniform within the cardiac wall, but rotates by as much as 180° throughout the wall thickness. Numerical simulations and experiments have indicated that this rotational anisotropy considerably affects the spread of excitation in cardiac tissue: the wave front shows a complex intramural shape with trailing cusps. The cusps can travel across layers and reach the epicardial and endocardial surfaces where they cause apparent accelerations of propagation. In the present study we provide an analytical description of the asymptotic wave front, as well as of cusp waves. We investigate the motion of cusp waves, based on the assumption that they occur at the intersection of asymptotic solutions, and we show that our theoretical analysis is in close agreement with numerical simulations. The asymptotic solutions are found to be determined purely by the fiber organization within the cardiac wall, independent of the excitable properties of cardiac tissue.

DOI: 10.1103/PhysRevE.70.061913 PACS number(s): 87.10.+e, 87.18.−h, 87.18.Bb

I. INTRODUCTION

The human ventricular myocardium consists of interconnected cardiac muscle cells, whose shape is usually approximated by a cylinder with a diameter of 10–20 μm and a length of 80–100 μm. These cardiac cells have more end-to-end connections than side-to-side connections [1], forming the muscle fibers. The electrical conductivity is much higher along than across the fibers, making the myocardium highly anisotropic [2]. The fibers show a helical arrangement throughout the ventricles, with a counterclockwise rotation of the fiber direction from the epicardial to the endocardial surface by 120° in the human heart [3] [Fig. 1(a)]. This has been called rotational anisotropy and the rotational angle is often assumed to have a linear dependence on depth within the ventricular wall [3].

Rotational anisotropy has been found to have profound implications on the propagation of electrical signals in cardiac tissue. Numerical simulations showed that fiber rotation could produce intramural trailing cusps [4,5] and complex epicardial activation patterns [6]. Figure 1(b) shows an example of the formation and disappearance of a cusp wave inside the myocardial wall. It depicts the intramural propagation (in the *xz* plane) of a wave induced by stimulation of the left bottom corner. Initially the wave front shows a regular concentric pattern. As the wave propagates into the upper layers, where the fibers are more aligned with the *x* axis [see Fig. 1(a)], the conduction velocity in the *x* direction increases. As a result, the upper portions of the wave front start propagating at higher velocities along the *x* axis and a trailing cusp is formed [indicated by a circle in Fig. 1(b)] where the local fiber orientation is perpendicular to the propagation direction. With time, the cusp moves across fiber layers. It eventually disappears at the epicardial surface, where it causes an apparent acceleration of propagation. These apparent accelerations have been observed in several experiments [7,8] and simulations [9]. Despite this qualitative understanding of the formation of cusp waves in cardiac tissue, the mechanisms underlying their motion across fiber layers remain unclear.

Figure 1(b) shows another interesting feature of intramural propagation: after the cusp has disappeared, the wave front acquires a stationary shape [indicated by an arrow in Fig. 1(b)] and propagates at a constant translational velocity in the *x* direction. Its leading peak is located in the upper layer where the fibers are parallel to the *x* axis. To date, this asymptotic behavior was only described in numerical simulations based on the eikonal-curvature equation [10,11]. So far, no study has provided a quantitative analysis of the asymptotic regime.

In this paper we derive a closed-form solution for the asymptotic wave front. We predict the motion of cusps across fiber layers, based on the assumption that cusps arise at the intersection of asymptotic solutions. We apply the theory to predict when and where such cusps vanish and, by

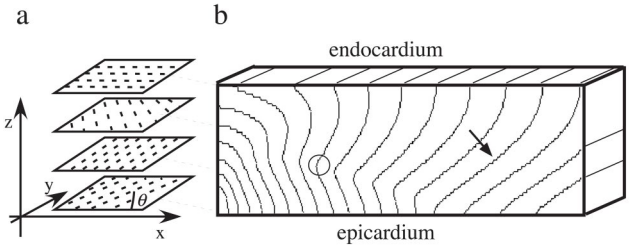

FIG. 1. Fiber rotation through the ventricular wall and intramural cusp waves. Panel (a) shows the counterclockwise rotation of the fibers (thick dashed lines) from epicardium to endocardium. It also depicts the associated coordinate system, with the *x* axis and the *y* axis parallel to the fiber layers and the *z* axis going from epicardium to endocardium. The fiber orientation in each layer is determined by the angle θ made with the *x* axis. Panel (b) shows an isochronal map illustrating the formation, motion, and disappearance of the cusp (indicated by a circle). The wave was initiated in the left bottom corner edge $(0,y,0)$. After the cusp disappears at the epicardial surface, a stationary wave is formed (arrow). Isochrones are plotted at 10-ms intervals, in a slab of 10 cm $\times$ 4 cm $\times$ 0.8 cm, with a total fiber rotation of $2\pi/3$ from bottom to top. The scale in the *z* direction was increased to make the waves more visible.

doing so, cause apparent accelerations on the epicardial or endocardial surface. Finally, we test our theoretical predictions in numerical simulations, using an ionic model of cardiac tissue [12].

II. GEOMETRY AND PROPAGATION MODEL

A portion of the ventricular wall and its constituting fiber layers is shown in Fig. 1(a). The coordinate normal to the layers is z, measured from the epicardial (outer) surface of the heart, while x and y are orthogonal coordinates along the layers. For the subsequent theoretical analysis, the boundaries in the x and y directions are irrelevant, and therefore, we assume the slab to be infinite in those directions.

Wave propagation is assumed to obey the standard monodomain reaction-diffusion equations

$$\partial_t u - \partial_i(D_{ij}\partial_j u) + \Phi(u,\vec{v}) = 0, \tag{1}$$

$$\partial_t \vec{v} + \epsilon\vec{\Psi}(u,\vec{v}) = 0. \tag{2}$$

where t is time and the spatial coordinates are $(x_1,x_2,x_3)=(x,y,z)$; in Eq. (1), a double sum over i and j is understood. The propagating variables are u (the transmembrane potential) and a set of additional variables $\vec{v}$, also called the gating variables. The reaction functions Φ and $\vec{\Psi}$ are in general nonlinear and represent the transmembrane ionic currents and their relaxation kinetics, respectively. The parameter ϵ adjusts the fast-time scale relative to the slower ones. At the two boundaries in the z direction, we require the standard no-flux condition $\partial_z u=0$, whose simple form is due here to the fibers being parallel to the surface.

The diffusivity matrix D encodes the geometry of Fig. 1(a). Its nonzero components are

$$D_{11} = D_L \cos^2\theta + D_T \sin^2\theta,$$

$$D_{22} = D_L \sin^2\theta + D_T \cos^2\theta,$$

$$D_{33} = D_T,$$

$$D_{12} = D_{21} = (D_L - D_T)\cos\theta \sin\theta, \tag{3}$$

where D_L and D_T are the diffusion coefficients along and across fibers, respectively, and where θ determines the fiber orientation in each layer [Fig. 1(a)]. We will assume linear rotational anisotropy—i.e.,

$$\theta = kz + \theta_1, \quad 0 \leqslant z \leqslant L \quad (k > 0, \theta_1 = \text{const}), \tag{4}$$

with L the thickness of the wall.

To represent the excitable dynamics of normal cardiac tissue in simulations—i.e., the functions Φ and $\vec{\Psi}$ in Eqs. (1) and (2)—we used a modification of the dynamic Luo-Rudy model (LRd) model [13] developed by Faber and Rudy [12]. The LRd model is a general mammalian ventricular cell model, mainly based on data obtained from the guinea pig. The model includes different ionic channel currents, represented mathematically by the Hodgkin-Huxley formalism [14], as well as ionic pumps and exchangers, and describes intracellular changes in ionic concentrations. Throughout this manuscript we will use the following parameter values, typical of human right ventricular tissue [15,16]: $k=2.6$ rad/cm, $D_L=1$ cm^2/s, and $D_T=0.11$ cm^2/s. For these values, the ionic model yields a longitudinal conduction velocity c_L of 65 cm/s and a transversal conduction velocity c_T of 22 cm/sec.

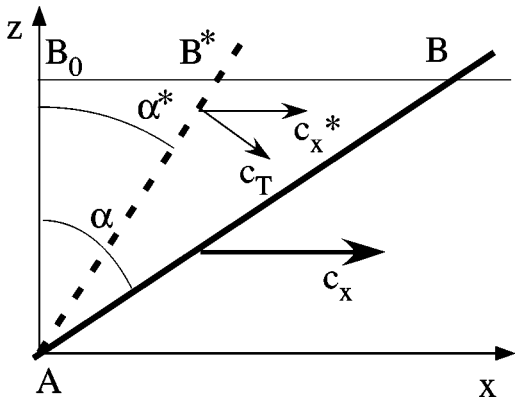

FIG. 2. Wave front segment in the normal (AB) and the isotropized (AB^*) medium. The angles with the z axis are denoted by α and α^*. The translational velocities c_x and c_x^*, as well as the velocity normal to the isotropized wave front (c_T), are shown.

Note that the detailed form of Φ and Ψ in Eqs. (1) and (2) is unimportant in the subsequent theoretical analysis. The specific dynamics of the model will affect the following considerations only through the parameter c_T.

III. ASYMPTOTIC WAVE PROPAGATION

A. Slope-driven front behavior

We study plane waves propagating in the x direction [see Fig. 1(b)]. We exploit the remaining y symmetry by assuming y-independent solutions. This initial condition breaks the helical symmetry of the slab described by Eq. (4). We assume the existence of an asymptotic steady-state solution, represented by a function $x=F(\theta)=F(kz+\theta_1)$, and propagating uniformly at a translational velocity c_x. In a medium where the conduction velocity along the x direction is different in each layer due to the fiber rotation, this can only be achieved for wave fronts with a specific tilt in each layer. In this section we derive an equation for the slope F' of the asymptotic wave front as a function of the fiber orientation in a given layer.

Consider an arbitrary slice of the wave front as depicted in Fig. 2, thin enough in the z direction so that the variation in θ can be neglected. The x-to-z anisotropy ratio ρ^2 inside this slice is

$$\rho^2 = \frac{D_{11}}{D_{33}} = \rho_0^2 - (\rho_0^2 - 1)\sin^2\theta, \tag{5}$$

where $\rho_0^2=D_L/D_T$; ρ and ρ_0 are positive.

In order to find the motion of front AB, we first "isotropize" the slice by scaling its x dimension by a factor $1/\rho$, in order to achieve an isotropic medium with diffusivity D_T. In

Fig. 2, let α be the angle between front AB and the z direction, while α^* is the corresponding angle, involving the isotropized front AB^*. The normal velocity to the front AB^* is c_T, which should equal $c_x^* \cos \alpha^*$ (Fig. 2). Knowing that the translational velocity scales as the x dimension, it is easily shown that

$$\tan^2 \alpha = (c_x/c_T)^2 - \rho^2. \tag{6}$$

Using $\tan \alpha = dF/dz = kF'(\theta)$, as well as Eq. (5), we get, from Eq. (6),

$$(F')^2 = \frac{1}{k^2}\left[\left(\frac{c_x}{c_T}\right)^2 - \rho_0^2 + (\rho_0^2 - 1)\sin^2 \theta\right]. \tag{7}$$

This equation describes a family of asymptotic solutions with translational velocities c_x. The value of c_x depends on the fiber organization in the slab and can be found from Eq. (7) (see next section).

B. Asymptotic shape and translational velocity

Consider a slab of tissue with a wave propagating in the x direction. The asymptotic wave front has a leading peak in the layer $\theta = \theta_{\min}$ where the fibers are the best aligned with the x axis—i.e., where θ is closer to 0 mod π [see Fig. 1(b) for example].

First, we calculate the translational velocity c_x from Eq. (7). If the leading peak occurs at one of the boundaries of the slab, we have $F' = 0$ due to the no-flux boundary condition. For a leading peak inside the myocardial wall, F' also equals 0, since it is an extremum of F. By substitution of $F'(\theta_{\min}) = 0$ in Eq. (7), we find the translational velocity

$$c_x(\theta_{\min}) = \sqrt{(c_L \cos \theta_{\min})^2 + (c_T \sin \theta_{\min})^2}, \tag{8}$$

where $c_L = c_T \rho_0$ and where we considered waves propagating in the positive x direction.

Next, we calculate the asymptotic shape of the wave front. Inserting the value of c_x from Eq. (8) into Eq. (7) and integrating from $\theta_{\min}$ to any point within the wall thickness, we find

$$F(\theta) = \frac{\sqrt{\rho_0^2 - 1}}{k}\sigma_{\pm}(\theta, \theta_{\min}) + F_0, \tag{9}$$

with F_0 an integration constant depending on the origin of the x axis and

$$\sigma_{\pm}(\theta, \theta_{\min}) = \pm \int_{\theta_{\min}}^{\theta} \sqrt{\sin^2 \theta' - \sin^2 \theta_{\min}}\, d\theta'. \tag{10}$$

The sign determines the slope of the front and is positive for $\theta < \theta_{\min}$ and negative for $\theta > \theta_{\min}$.

C. Frequent case

Usually, fibers rotate by at least $2\pi/3$ throughout the ventricular wall [3]. It is therefore common to have a fiber parallel to the x axis at a certain depth. In this case—i.e., $\theta_{\min} = 0$—Eq. (9) reduces to the more simple form

$$F(\theta) = \frac{\sqrt{\rho_0^2 - 1}}{k} \cos \theta + F_0. \tag{11}$$

The overall sign is chosen for a convex front. Returning to Eq. (8) and setting $\theta_{\min} = 0$ we find

$$c_x = c_L. \tag{12}$$

Remarkably and consistently with numerical simulations performed by Keener and Panfilov [5], the translational velocity is entrained to the longitudinal conduction velocity c_L over the whole wall thickness even, for example, where the local fibers are perpendicular to the translational motion.

Although Eq. (11) is a special case of Eq. (9), we will refer to them as cosine and elliptic integral wave solutions, respectively.

IV. QUASIASYMPTOTIC REGIME: CUSP WAVES

An initially plane wave front will go through a transient phase before reaching its asymptotic regime. It will become wavy, as the conduction velocity is different in each fiber layer. If there is a layer where the fibers are perpendicular to the propagation direction, a trailing cusp will be formed as a result of the low conduction velocity. The wave front has two leading peaks, one above and one under the cusp, propagating a their own velocities [see Fig. 1(b)]. In this section we derive the quasiasymptotic kinetics of cusp waves, based on the assumption that cusps occur at the intersection of two asymptotic solutions, each described by Eq. (9).

Consider a slab with boundaries at $\theta = \theta_1$ (epicardium) and $\theta = \theta_2$ (endocardium). For simplicity, we take $0 \leqslant \theta_1 < \theta_2 \leqslant \pi$. Assume a layer with fibers perpendicular to the x axis, where a cusp is formed in an initially plane wave front. This layer splits the wave front into two portions, a lower one, represented by the function x_1, and one above the cusp, represented by x_2. We assume that x_1 and x_2 are independent solutions of Eq. (7) with a cusp at their intersection. The solution x_1 has a leading peak at $\theta = \theta_1$ and the solution x_2 at $\theta = \theta_2$. The quasiasymptotic kinetics are described by

$$x_1(\theta, t) = f\sigma_+(\theta, \theta_1) + F_{0,1} + c_x(\theta_1)t,$$

$$x_2(\theta, t) = f\sigma_-(\theta, \theta_2) + F_{0,2} + c_x(\theta_2)t, \tag{13}$$

with $f = (\sqrt{\rho_0^2 - 1})/k$. The integration constants $F_{0,1}$ and $F_{0,2}$ can be found by fixing the origin of the x axis. We chose the cusp to be located at $x = 0$ at time $t = 0$. Substitution into Eqs. (13) yields, for a cusp in the layer $\theta = \pi/2$,

$$F_{0,1} = -f\sigma_+\left(\frac{\pi}{2}, \theta_1\right), \quad F_{0,2} = -f\sigma_-\left(\frac{\pi}{2}, \theta_2\right). \tag{14}$$

Note that cusps can, for example, also be formed where two asymptotic wave fronts collide. This does not necessarily have to be in the layer $\theta = \pi/2$ and will, therefore, affect the value of the integration constants in Eq. (14). The subsequent analysis is, however, valid for such cusps as well.

A. Vanishing cusps

If $|\theta_1 + \theta_2| \neq \pi$, the translational velocities $c_x(\theta_1)$ and $c_x(\theta_2)$ are different. In this case, the faster portion of the

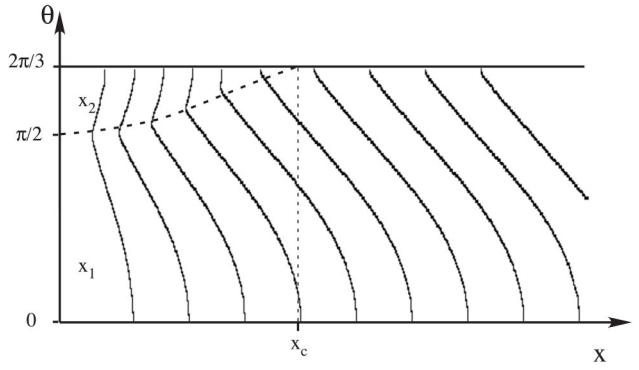

FIG. 3. Schematics of the motion of a trailing cusp (thick dashed line) at the intersection of two quasiasymptotic solutions x_1 and x_2, for $\theta_1=0$ and $\theta_2=2\pi/3$. The cusp reaches the surface $\theta=\theta_2$ at a distance x_c.

wave front will gradually overtake the slower one. As a result, the cusp will move towards one of the tissue boundaries, where it eventually disappears (see Fig. 3). Whenever this occurs, an apparent acceleration of the wave front will be observed on that surface: as the faster portion reaches the surface, the translational velocity in the x direction suddenly increases. For example, if $\theta_1<\theta_2$ mod π, the portion x_1 will have a larger translational velocity and the cusp will disappear at the surface $\theta=\theta_2$. The time t_c at which the cusp will reach that layer can be found by solving Eqs. (13) for t:

$$t_c=\frac{1}{c_x(\theta_1)-c_x(\theta_2)}[-f\sigma_+(\theta_2,\theta_1)+F_{0,2}-F_{0,1}]. \quad (15)$$

The distance x_c at which the cusp reaches the surface $\theta=\theta_2$ (Fig. 3) is then given by

$$x_c=x_1(\theta_2,t_c)=x_2(\theta_2,t_c)=F_{0,2}+c_x(\theta_2)t_c, \quad (16)$$

where $F_{0,1}$ and $F_{0,2}$ are given by Eq. (14). The equations for a cusp disappearing at the surface $\theta=\theta_1$ are similar. Note that the same approach can be used to determine the time and location at which the cusp crosses an arbitrary layer within the myocardial wall.

B. Nonvanishing cusps

If $|\theta_1+\theta_2|=\pi$, both portions of the wave front have the same translational velocity. In this case, the cusp remains in the same fiber layer indefinitely and the quasiasymptotic regime described by Eqs. (13) is an asymptotic one, different from the solution derived previously, as it now shows a cusp.

V. CURVATURE EFFECTS

It is well known that in reaction-diffusion media such as cardiac tissue, the curvature of a wave front will affect its propagation velocity: if the front is concave, it will propagate faster than if it is convex. To what extent is our neglect of curvature justified? The question is most conveniently answered in the isotropized medium, with diffusivity D_T.

First, we focus on the leading peak. We take a cosine wave as an illustration. In order to obtain an estimate of the curvature effects we consider a thin slice around the leading peak at $\theta=0$, in which fiber rotation can be neglected. In the isotropized medium, the eikonal relation for this thin slice reads

$$c_x^*=c_T-D_T\mathcal{K}^*, \quad (17)$$

where $\mathcal{K}^*$ is the curvature of the front.

The curvature is given by the second derivative of the isotropized front, $\mathcal{K}^*=d^2F^*(\theta)/dz^2$, or, in terms of the slope,

$$\mathcal{K}^*=\frac{d(\tan\alpha^*)}{dz}=\frac{d}{dz}\frac{\tan\alpha}{\rho}. \quad (18)$$

Thus we get

$$\mathcal{K}^*=k^2\frac{d}{d\theta}\frac{F'(\theta)}{\rho} \quad (19)$$

$$=k^2\left[\frac{F''(\theta)}{\rho}+F'(\theta)\frac{d}{d\theta}\frac{1}{\rho}\right]. \quad (20)$$

At $\theta=0$, we have $F'=0$ as well as $(d/d\theta)(1/\rho)=0$. Hence, we get

$$\mathcal{K}^*=k^2\frac{F''(0)}{\rho(\theta=0)}=\frac{k\sqrt{\rho_0^2-1}}{\rho_0} \quad (21)$$

after using Eqs. (5) and (11) and taking the sign for positive curvature. From Eq. (21), we have $K^*=5.2\sqrt{2}/3\approx 2.4$. Equation (17) becomes $c_x=22-0.26$, yielding a 1% curvature correction to the isotropized speed of the leading peak and, hence, also to its actual speed. Note that in the left ventricle, k is even smaller ($\sim$1.3 rad/cm), yielding an even smaller curvature correction. We conclude that curvature has little effect on the propagation of the cosine wave.

We next consider a trailing cusp. Here the converse approach is informative: knowing what speed correction is needed, we estimate the curvature and judge to what extent the cusp is an imperfect one. By way of illustration we examine the symmetric case where $\theta_1=0$, $\theta_2=\pi$. The cusp is at middepth, $\theta=\pi/2$, where the medium is already isotropic. However, the overall asymptotic wave moves rigidly in the x direction at speed c_L.

At its leftmost point, the cusp must have a slope $dF/dz=0$. Without any curvature correction, its speed would simply be c_T. Therefore we need a correction c_L-c_T. Such a large correction, twice the original speed, may be too extreme for us to put much trust in the eikonal equation. However, if we persist, we now have, instead of Eq. (17),

$$c_L=c_T-D_T\mathcal{K}. \quad (22)$$

Therefore we obtain the concave curvature

$$\mathcal{K}=\frac{c_T-c_L}{D_T}=\frac{c_L}{D_T}\left(\frac{1}{\rho}-1\right) \quad (23)$$

or, in cm^{-1}, $\mathcal{K}=(65)(9)(1/3-1)=-396$, corresponding to a radius of curvature $r\approx-0.0025$ cm. For comparison, the inverse pitch is $k^{-1}=0.38$ cm and the wave front in human

cardiac tissue is usually 0.2 cm thick. Mathematically speaking, a cusp has infinite curvature or, equivalently, a radius of curvature equal to zero. Here, the radius of curvature is much smaller than any other spatial dimension of interest, and therefore, the cusp is perfect for practical purposes.

VI. THEORY VERSUS COMPUTATIONS

In the simulations, we have considered slabs of cardiac tissue with dimensions 6 cm $\times$ 6 cm $\times$ 0.8 cm, to mimic a typical portion of the right ventricular wall. To integrate Eq. (1) we have used the operator splitting method to split it into an ordinary differential equation (ODE) for the reaction part Φ and a partial differential equation (PDE) for anisotropic diffusion. The ODE was solved using a forward Euler scheme with a time step of 0.01 ms. The relaxation equations (2) of the gating variable in the LRd model were integrated using a technique presented by Rush and Larsen [17]. The diffusion PDE was also solved using a forward Euler scheme with a space step of 0.10 mm, yielding a numerical accuracy of more than 95% with respect to the conduction velocity of action potentials. In the simulations, no-flux boundary conditions were assumed for all boundaries. All simulations were coded in the C++ programming language and computations were carried out on a parallel cluster consisting of 16 nodes equipped with dual AMD Athlon MP 2200+ processors running at 1.8 GHZ. Each node has 1 GB of RAM with the exception of the master node that has 4 GB. We used the MPI library and a simple "domain slicing" algorithm [18] to parallelize the code.

For the fiber organization we have addressed two different cases: in case 1 we put $\theta_1=0$ and $\theta_2=2\pi/3$ and in case 2 we had $\theta_1=5\pi/18$ and $\theta_2=17\pi/18$. For both cases we compare the asymptotic shape and translational velocity in theory and simulation, as well as the motion of cusps.

A. Shape and translational velocity of the asymptotic wave front

For case 1 the theoretical asymptotic solution is given by a cosine wave propagating at the longitudinal velocity of 65 cm/s. In our numerical simulations we found an asymptotic wave front propagating at 64.7 cm/s, which deviates less than 1% from the theoretically predicted value. In Fig. 4(a) we compare the shape of the "surviving" asymptotic wave in the simulation with the theoretically predicted cosine wave. We see that theory and simulation are in close agreement.

For case 2, the theory predicts an elliptic integral wave moving at a speed $c_x=62.8$ cm/s, as obtained from Eq. (8). Our computations show an asymptotic wave propagating at 62.1 cm/s, again close to the theoretical value (about 1% deviation). Figure 4(b) compares the shape of the asymptotic simulated wave front and the theoretical shape obtained from elliptic integrals. Both curves show an almost perfect match.

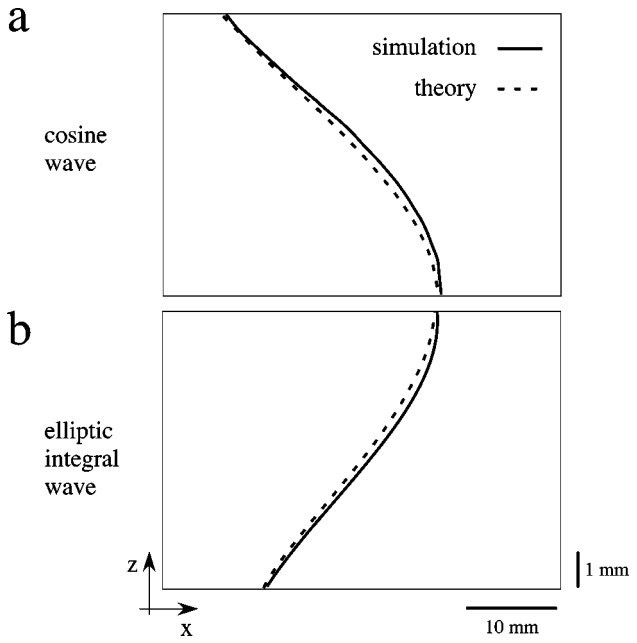

FIG. 4. Comparison of the asymptotic wave front in theory and simulations in case 1 (a) and case 2 (b).

B. Quasiasymptotic regime: Cusp waves

In this section we focus on the motion of cusps and the distance and time at which they reach one of the surfaces of the ventricular wall. As expected, our simulations show a cusp forming in both cases at $\theta=\pi/2$. In the first case the cusp eventually reaches the endocardial surface, where it causes a sudden increase in the translational velocity c_x. In the other case, a similar situation is observed, but on the epicardial surface. Figures 5(a) and 5(b) illustrate these observations. For each case we show intramural isochronal maps, depicting the formation and motion of the cusp. In both cases an arrow indicates the place where the cusp reaches the epicardial or endocardial surface.

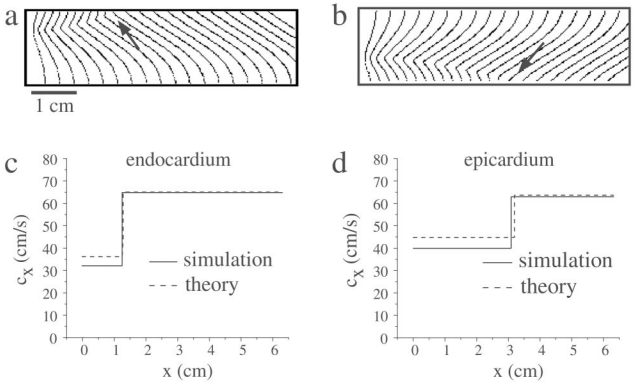

FIG. 5. Formation and disappearance of intramural cusp waves and its effect on the translational velocity c_x. We show transmural isochrones in the *xz* plane obtained in simulations for case 1 (a) and case 2 (b). The point where the cusp disappears at one of the surfaces is indicated by an arrow. Plots of the translational velocity c_x, on the endocardial surface for case 1 (c) and on the epicardial surface for case 2 (d), are shown as a function of x. Simulation (solid line) and theory (dashed line) are compared.

TABLE I. Time t_c and location x_c of cusps reaching the epicardial or endocardial surface: theory vs simulation.

		Theory	Simulation
Case 1	t_c (ms)	27	31
	x_c (cm)	1.23	1.20
Case 2	t_c (ms)	59	65
	x_c (cm)	3.03	2.93

The theory enables us to predict the time and location of the sudden increase in c_x, by Eqs. (15) and (16). First we need to determine the integration constants and the translational velocities. For case 1, we found $F_{0,1}=0$ cm and $F_{0,2}=0.22$ cm [by numerical integration of Eq. (14)]. For the cosine wave with leading peak at $\theta=0$ the translational velocity is $c_x(\theta_1)=65$ cm/s. The translational velocity $c_x(\theta_2)$ of the elliptic integral wave is readily found from Eq. (8) and has the value 37.52 cm/s. For the second case, the integration constants are $F_{0,1}=0.37$ cm and $F_{0,2}=1.03$ cm, whereas the translational velocities were found to be 44.9 cm/s $[c_x(\theta_1)]$ and 62.8 cm/s $[c_x(\theta_2)]$.

Table I compares the time and location of the disappearance of the cusps in simulation and theory, for both cases. For the theory, we evaluated the remaining unknown term $\sigma(\theta_2,\theta_1)$ in Eq. (15), by numerical integration. Note that, in the theoretical considerations of Sec. IV, we have assumed that the cusp was fully formed at $t=0$. In reality, it takes some time before such cusps develop in an initially plane wave front. Therefore, in the simulations, we waited 20 ms after stimulating the plane $x=0$, in order for a cusp to form in the wave front (fourth isochrone in Fig. 5 for each setup). From Table I we conclude that the theory predicts for both cases a smaller t_c than seen in the simulations. Theoretical and computed values are, however, always close (about 10% deviation). Moreover, the error in the location x_c is for both setups less than 5%. Again, we conclude that theory and simulations are in close agreement.

Figures 5(c) and 5(d) show the translational velocity on the endocardial surface for case 1 [Fig. 5(c)] and on the epicardial surface for case 2 [Fig. 5(d)], as a function of x. The results obtained from the simulation are shown as a solid line, while the theoretical curve is depicted as a dashed line. As expected, a sudden increase of translational velocity was observed, when the cusp reached the surface of interest. In both cases, the simulations yield a lower translational velocity (by about 10%), before the sudden increase. After the cusp has disappeared on one of the outer surfaces, we see that theory and simulation show an almost perfect match (about 1% deviation; see Sec. VI B).

VII. DISCUSSION

To date, the asymptotic wave propagation in cardiac tissue was only studied in numerical simulations. In this paper, we have presented an analytical description of the intramural propagation in cardiac tissue. We have derived the shape and translational velocity of the asymptotic wave front. We found, in accordance with earlier simulation studies [4,5], that the asymptotic waves propagate at the speed calculated along the best aligned fibers. We have studied the quasiasymptotic regime where trailing cusps are present. The motion of cusps was studied, based on the assumption that they occur at the intersection of two asymptotic wave solutions. If those solutions have different translational velocities, the cusp gradually moves toward the endocardial or epicardial surface, where it causes apparent accelerations of the wave front. Knowing when and where such accelerations occur is of experimental relevance, for example when trying to determine the longitudinal and transversal propagation velocities in cardiac tissue. We apply the theory to predict the location and time at which such accelerations occur. Simulations were performed in an extensive model of ventricular tissue. We show that the theory is in close agreement with the numerical computations and can be used as a predictive tool.

Throughout this manuscript we have assumed linear rotational anisotropy, described by Eq. (4), based on experimental evidence [15,19]. Some experimental studies have, however, shown a nonlinear dependence on the depth coordinate z in the pulmonary conus [7] and in epicardial layers of the swine right ventricle [20]. We believe that our theoretical approach is general enough to allow the use of any function $\theta(z)$. This will of course affect the shape of the asymptotic wave fronts, which, depending on the choice of $\theta(z)$, might no longer be described by cosine or elliptic integral waves. The main results of our study with respect to cusp waves and apparent accelerations on the outer surfaces will, however, remain unaffected.

We have used a monodomain approach for the reaction-diffusion properties of cardiac tissue, neglecting its bidomain structure consisting of intracellular and extracellular media. The bidomain properties have been shown to play a role in the formation of virtual electrodes close to the site of stimulation [21]. In the present paper, we were, however, interested in propagation far from the stimulating electrode. Therefore we believe that the incorporation of bidomain kinetics is likely to have little or no effect on the results of this study.

Surprisingly, curvature effects were shown to play a negligible role in the developed analysis. The asymptotic wave front propagates at the speed along the best aligned fiber, independent of its curvature. This result should not be taken for granted, however. Equation (21) indicates that a sufficient increase in the pitch k would make the effect noticeable. This could be the case in some smaller animal hearts, where the total fiber rotation can be up to 180° [22], whereas the wall thickness can be much smaller than 0.8 cm.

Our analysis is essentially a geometrical one, without any assumption of the choice of ionic model. It is reasonable to assume that it will hold for any type of cardiac model.

ACKNOWLEDGMENTS

The authors would like to thank Dr. C. Zemlin for assistance on the simulation part and Dr. O. Berenfeld for a helping hand on Fig. 1. This research was supported by NIH Grants No. 5R01HL071635 and No. 5R01HL071762.

[1] R. Hoyt, J. Cohen, and J. Saffitz, Circ. Res. **64**, 563 (1989).
[2] L. Clerc, J. Physiol. (London) **255**, 335 (1976).
[3] D. Streeter, *Handbook of Physiology* (American Physiological Society, Bethesda, MD, 1979), Sec. 2, Vol. I, pp. 61–112.
[4] J. Keener and A. Panfilov, J. Cardiovasc. Electrophysiol. **4**, 412 (1993).
[5] J. Keener and A. Panfilov, in *Cardiac Electrophysiology: From cell to bedside*, 2nd ed., edited by D. P. Zipes and J. Jalife (Saunders, Philadelphia, 1995), pp. 335–347.
[6] P. Colli-Franzone, L. Guerri, M. Pennacchio, and B. Taccardi, Math. Biosci. **147**, 131 (1998).
[7] M. Burgess, B. Steinhaus, K. Spitzer, and P. Ershler, Circ. Res. **62**, 233 (1988).
[8] B. Taccardi, R. Lux, P. R. Ershler, S. Watabe, and E. Macchi, in *Advances in Electrocardiology*, edited by Z. Antaloczy (Elsevier, Amsterdam, 1990), pp. 61–62.
[9] A. Pollard, M. Burgess, and K. Spitzer, Circ. Res. **72**, 744 (1993).
[10] P. Colli-Franzone, L. Guerri, and S. Tentoni, J. Math. Biol. **28**, 121 (1990).
[11] J. Keener, J. Math. Biol. **29**, 629 (1991).
[12] G. Faber and Y. Rudy, Biophys. J. **78**, 2392 (2000).
[13] C. Luo and Y. Rudy, Circ. Res. **74**, 1071 (1994).
[14] A. Hodgkin and A. Huxley, J. Physiol. (London) **117**, 500 (1952).
[15] D. Streeter, M. Spotnitz, D. Patel, J. Ross, and E. Sonnenblick, Circ. Res. **24**, 339 (1969).
[16] P. Taggart, P. Vetter, T. Opthof, R. Coronel, R. Trimlett, W. Pugsley, and P. Kallis, J. Mol. Cell. Cardiol. **32**, 621 (2000).
[17] S. Rush and H. Larsen, IEEE Trans. Biomed. Eng. **25**, 389 (1978).
[18] R. Zaritsky, and A. Pertsov, in *Proceedings of Neural, Parallel and Scientific Computations*, edited by M. Bekakos, G. Ladde, N. Medhin and M. Sambandham (Dynamic, Atlanta, 2002), Vol. 2, p. 187.
[19] J. Armour and W. Randall, Am. J. Physiol. **218**, 1517 (1970).
[20] S. Simons, F. Vetter, S. Mironov, C. Hyatt, and A. Pertsov, J. Physiol. (London) **544P**, S147 (2002).
[21] B. Roth, J. Cardiovasc. Electrophysiol. **8**, 768 (1997).
[22] D. J. Streeter and D. Bassett, Anat. Rec. **155**, 503 (1966).